Egyptian Journal of Soil Science

http://ejss.journals.ekb.eg/

PRISMA-Driven Hyperspectral Analysis for Characterization of Soil Salinity Patterns in Sohag, Egypt

Ali R. A. Moursy[1], Moatez A. El-Sayed[2], Mohamed E. Fadl[3] and **Alaa H. Abd-Elazem[4*]**

[1]*Soils and Water Department, Faculty of Agriculture, Sohag University, Sohag 82524, Egypt*
[2] *Soils and Water Department, Faculty of Agriculture, Al-Azhar University, Assiut 71524, Egypt*
[3]*Division of Scientific Training and Continuous Studies, National Authority for Remote Sensing and Space Sciences (NARSS), Cairo 11769, Egypt, Adhamnarss@yahoo.com*
[4]*Soil and Natural Resources Department, Faculty of Agriculture and Natural Resources, Aswan University, Aswan 81528, Egypt*

SOIL salinization is a major environmental issue in Egypt's semi-arid region, characterized by low precipitations rate, high temperatures, and high evaporation rates, ultimately lowers agricultural sustainability. Consequently, effective soil salinity observation, evaluation and mapping are vital to mitigate the negative impacts of soil degradation and ensure sustainable land management. Therefore, this study focused on estimating and mapping soil salinity in semi-arid lands (Sohag Governorate, Egypt), using PRISMA (PRecursore IperSpettrale della Missione Applicativa) visible-Near-Infra-Red (vis-NIR) hyperspectral images as an advanced tool that offers significant promise for extracting detailed information about the composition and condition of the observed areas. For this study, seventeen representative soil profiles were collected in more than 150 cm depth from the field and subsequently analyzed in the lab to determine their EC (dS/m) values. Moreover, PRISMA hyperspectral image of the investigated area was acquired, processed, and some soil salinity hyperspectral indices were applied such as; Salinity Index (SI), Brightness Index (BI), Normalized Differential Salinity Index (NDSI), Combined Spectral Response Index (COSRI) and Coloration Index (CI). Among the PRISMA hyperspectral image, six bands were significant (12, 23, 25, 31, 32, and 49) and used for calculating the hyperspectral indices. Soil salinity spatial variability maps of the study area were generated using the relation between the developed hyperspectral indices and the observed soil salinity as EC values (dS/m). The study area demonstrated a relatively consistent level of salinity, with soil EC values ranging from 0.9 to 2.10 dS/m and averaging 1.40 dS/m, this moderate salinity, evident in the generated maps, suggests a relatively stable soil condition. The COSRI and CI hyperspectral salinity indices achieved the highest accuracy in estimating soil salinity (EC) with coefficient off determination (R^2) values of 0.68 and 0.64 , respectively; and the root mean square error (RMSE) values were 0.26 and 0.29 dS/m, respectively. Other indices such as; normalized difference vegetation index (NDVI), NDSI, BI, and SI had lower capability for estimating soil salinity over the study area. The PRISMA hyperspectral data is a very potential tool for estimating soil salinity in the studied area, therefore, monitoring and analyzing soil salinity are essential for developing effective land management strategies.

Keywords: Soil salinity, PRISMA image, hyperspectral data, soil indices.

1. Introduction

Soil salinity in Sohag Governorate, Egypt, poses a major challenge to agricultural productivity and land use, driven by both natural and human factors. Naturally, irrigation water from the Nile River contains dissolved salts, which contribute to soil salinity. In addition, the region's high temperatures and low rainfall promote rapid evaporation, which leads to salts concentration. Human activities exacerbate these problems through excessive irrigation without proper drainage, which leads to salt accumulation. Furthermore, poorly designed drainage systems impede the leaching of excess salts from the soil profile, while the improper use of chemical fertilizers

*Corresponding author e-mail: a.hashem@agr.aswu.edu.eg
Received: 07/08/2024; Accepted: 16/10/2024
DOI: 10.21608/EJSS.2024.310679.1836

exacerbates soil salinity concerns (Fadl et al. 2023). In Sohag Governorate, several soil related challenges have emerged due to urbanization, population growth, and other factors. A significant problem of the agricultural soils is the wastewater impact on clayey soils; whereas in Upper Egypt, regions situated on floodplain clayey soils (composed of silts, clays, and sands) near the River Nile have faced considerable difficulties (Moursy and Thabit 2022). Additionally, the lack of sewage networks in newly developed areas necessitates private wastewater storage in tanks located beneath or near houses. When these tanks overflow or rupture, the organic-rich wastewater infiltrates the clayey soils, increasing their plasticity and swelling potential, this has led to significant damage, including wall cracks and foundation tilting (Negim and Moursy 2023). Another issue is an urban sprawl and soil deterioration; whereas population growth has led to urban sprawl, resulting in the loss of old agricultural soils in Sohag Governorate. Furthermore, maximizing land resource utilization is crucial to mitigate the effects of soil degradation. The land cover change and fertile land loss is significant problem in agricultural soils of Sohag (Abdel-rahman and Negim 2016). Furthermore, the conversion of fertile lands into urban settlements has adversely affected soil quality and another significant issue concerns groundwater salinization and soil salinity, with groundwater salinity levels increasing over the past 15 years, thereby impacting soil layersby leading to the accumulation of salts, increasing electrical conductivity, and altering soil structure. This results in higher salinity levels, particularly in surface layers, and can cause degradation of soil fertility through processes like sodicity, which reduces water infiltration and root penetration (El-Aziz et al., 2024). Consequently, these changes pose serious challenges to agricultural productivity, necessitating effective management practices to monitor salinity and maintain soil health for sustainable land use (Wang et al., 2024). Moreover, soil salinity has shown an upward trend from 1991 to 2006, particularly within specific categories, strongly saline soils (ECe = 10 dS/m) and extremely saline soils (ECe = 50 dS/m) as studied by Abd El-Aziz et al.(2018). Another challenge in Sohag soils is zinc contamination; exacerbated by increased clay content due to industrial, sewage, and Nile-irrigated activities whereas the clay minerals can interact chemically with zinc ions, potentially forming complexes that may increase the bioavailability of zinc to plants and microorganisms (Wang et al., 2024). The specific mineral composition of the clay affects these interactions; for instance, certain clays may enhance the solubility of zinc under specific pH conditions, leading to greater mobility and availability in the soil (Seifollahi-Aghmiuni et al., 2022). This alteration affects the solubility of Zn^{2+} in the soil. Addressing these issues underscores the significance of adopting sustainable soil management implementations and enhancing environmental awareness to maintain soil health in Sohag Governorate (Ibrahim et al., 2021).

The effects of soil salinity significantly impact crop yield reduction by hindering plant growth, nutrient uptake, and water balance, whereas, salinity stress leads to decreased crop productivity (Rafie, 2024). Additionally, high salt concentrations degrade soil structure, reducing porosity and aeration. This renders land unsuitable for agriculture, affecting livelihoods and saline soils, characterized by elevated soluble salt levels in both surface and root zones, pose a threat to soil health and productivity. Soil salinization can lead to reduced productivity, unstable soil, lower water availability, and diminished biodiversity (Jalali et al., 2021). Salinization is prevalent in arid and semi-arid regions and tends to vary in distribution. Apart from natural processes such as, rock weathering, rainfall, and human activities also contribute significantly to soil salinity in these regions (Hassani et al., 2020; Ghanbari et al., 2023). Soil salinity provide as a crucial indicator when assessing soil salinization, which exhibits significant variation over time and across different locations (Zaman et al., 2018). Traditional methods for monitoring soil salinization, such as particular-point soil surveys followed by estimation of soil salinity paremetrs in laborotry analysis, which are labour-intensive and time- consumpting . Unfortunately, their slow update cycles do not align with the need for rapid acquisition of large-scale soil salinity data (Shepherd et al., 2002).

Hyperspectral remote sensing significantly impacts soil research by providing detailed spectral information. It enables rapid, non-destructive monitoring of soil nutrients, including moisture levels, nitrogen content, and organic matter (Lassalle et al., 2023). Through detailed spectral recordings, hyperspectral techniques facilitate the prediction of various physio-chemical and biological soil characteristics. These techniques can differentiate between bacterial and fungal influences on soil by analyzing specific chemical indicators and utilizing machine learning algorithms to classify soils based on their spectral data. Studies have demonstrated the effectiveness of

hyperspectral imaging in assessing soil attributes, such as organic compounds and nutrient levels, which vary according to microbial activity (Shen et al., 2020). Overall, hyperspectral methods provide a robust framework for understanding soil health and informing sustainable land management practices by revealing the intricate relationships between soil composition and microbial processes (Ewing et al., 2020). Researchers leverage this richness of data to enhance sustainable resource management and informed decision-making. Ultimately, hyperspectral remote sensing enhances agricultural practices and environmental management by providing deeper insights into soil composition and ecosystem dynamics (Cao et al., 2023).

Hyperspectral indices such as Salinity Index (SI), Brightness Index (BI), Normalized Differential Salinity Index (NDSI), Combined Spectral Response Index (COSRI) and Coloration Index (CI) are effective tools for soil salinity assessing and mapping, facilitating monitoring and informed land management strategies. For instance, Ferna´ndez-Buces et al. (2006) utilized COSRI and NDVI indices to establish a correlation between soil salinity and these indices. Numerous studies have employed hyperspectral indices to estimate and map various soil properties. Among these studies, Hu et al. (2019) used the un-manned aerial vehicle and hyperspectral satellite image for estimating and mapping soil salinity in some Chinese soils with R^2 values between 0.81 and 0.94. Gorji et al. (2017) found that the Hyperion (EO-1) hyperspectral image was better than Landsat 8 (OLI) multispectral image for estimating soil salinity in Mediterranean countries. Hamzeh et al. (2016) assessed the precision of hyperspectral (Hyperion1) and multispectral (Landsat 7) satellite images for schematic diagram of quantitative classification of salinity stress in some Iranian sugarcane fields, and they found that, the best performance of predicting and mapping soil salinity was recorded for the hyperspectral data.

PRISMA hyperspectral imagery (PHSI) is an instrumental widely used in soil research due to its high spectral resolution (≤12 nm) which allows precise analysis of soil physical and chemical properties. PHSI applications include vegetation mapping, soil mineral identification, and nutrient deficiency diagnosis. Challenges associated with PHSI include limited data availability, noisy bands, atmospheric interference, and computational demands. Despite these challenges, researchers can utilize PHSI for large-scale soil mapping and technology dissemination. Overall, PHSI significantly advances soil research by providing detailed spectral data that supports various applications (Shaik et al., 2023). In this research our study primarily aims to: (i) to characterize the soil salinity status in a specific area Sohag Governorate, Egypt; (ii) to estimate soil salinity using PRISMA hyperspectral image integrated with various soil salinity hyperspectral indices; and (iii) to map soil salinity across the investigated area.

2. Materials and methods

Figure 1 provides a visual representation of the materials and methods employed in this study, which depicts the experimental setup used to evaluate the effects of varying salinity levels. Soil samples were collected and analysed for the EC values. A PRISMA hyperspectral image was obtained which had the approximate date of soil sampling, the correlation between soil salinity hyperspectral indices and observed soil salinity (EC) values was assessed by applying the indices to the image, utilizing thesis indices, soil salinity maps were successfully generated for the studied area providing a valuable tool for assessing salinity distribution and its potential impacts.

2.1. Description of the study area

The research focuses on the area situated in the Sohag Governorate along the Nile River within the Nile Valley, where old agricultural alluvial soils, Figure (2). Sohag experiences a Subtropical Dry Arid (Desert) climate characterized by long, hot summers with scorching temperatures and clear skies. Winters in Sohag are relatively short, cool, dry, and mostly clear, with minimal snowfall or freezing conditions. Temperature typically varied from 7.8°C to 43.3°C (rarely dipping below 5°C or exceeding 43.3°C), and hot days are common throughout the year in Sohag.

2.2. Soil sampling and determination

Seventeen georeferenced soil profiles were gathered from the investigated area, concentrating on the topsoil's where salt accumulation is typically highest. The air-dried soil samples were passed through a 2mm sieve to ensure consistency for subsequent analysis. Soil reaction (pH) was measured in 1: 2.5 of soil to water suspension at 25 °C using a glass electrode as reported by **Alvarenga et al. (2012)**. According to **Bashour and Sayegh (2007)** soil paste extracts were analyzed for electrical conductivity (EC, dS/m) using an EC meter device as part of a comprehensive assessment of soil salinization in the study area. Total calcium carbonate ($CaCO_3$) was determined using Scheibler's calcimeter **(Nelson, 1982)**. Soluble anions: carbonates and bicarbonates were determined by the titration with a standard solution of hydrochloric acid, chlorides were determined using a standard solution of silver nitrate and sulphates were spectrophotometry measured using the turbidmetery method **(Jackson, 1973).** Soluble cations: Calcium and magnesium were determined using the titration with a standard versenate (EDTA) solution, while sodium and potassium were measured using the flamephotometery method **(Jackson, 1973)**. Sodium adsorption ratio (SAR_e) of saturated soil past extract was calculated using this equation that described by **Richards (1954)**. Cation exchange capacity (CEC) was measured using 1 M sodium acetate (NaOAc) solution (pH 8.2) as a saturation solution and then exchangeable (Na^+) was replaced by NH_4^+ using 1 M ammonium acetate (NH_4OAc) solution (pH 7.0) outlined by **Bashour and Sayegh (2007)**.

2.3. PRISMA image acquisition and pre-processing

Before conducting field surveys and soil sampling, a freely available PRISMA image dated September 23, 2023, was obtained from the Italian Space Agency (ASI) website (http://prisma.asi.it/missionselect/), launched on March 22, 2019, with spectral range between 400 to 2500 nm. The primary mission objective was for high-resolution hyperspectral imaging with a spatial resolution of 30m, and a swath width of 30 km, operates at an altitude of 614 km. The image was initially processed in the ENVI 5.3 software, where a format conversion algorithm was applied to stack its 173 spectral bands (66 in visible-Near Infrared (vis-NIR) and 107 in Near Infrared-Shortwave Infrared (NIR-SWIR)). It underwent atmospheric and geometric correction to enhance its quality (Figure 3.a) and was subsequently visualized as a false colour composite (FCC) (Figure 3.b). To focus specifically on the investigated area, the satellite image was masked using the study area border, resulting in the creation of a subset image (Figure 3.d). Both the full scene and the resized images were then subjected to a supervised classification process to delineate different land use and land cover (LULC) units within the research site. The resulting classified PRISMA images, representing both the entire scene and the study area subset, were presented in Figures 3.c and 3.e. Notably, areas depicted in brown indicate the presence of bare soil, which was identified as suitable for surveying and sampling purposes.

2.4. Soil hyperspectral data acquisition

Hyperspectral soil reflectance data from the soil samples were extracted from the stacked and rescaled PRISMA image of the study area utilizing the region of interest (ROI) tool which integrated in an environment of ENVI 5.3 software.

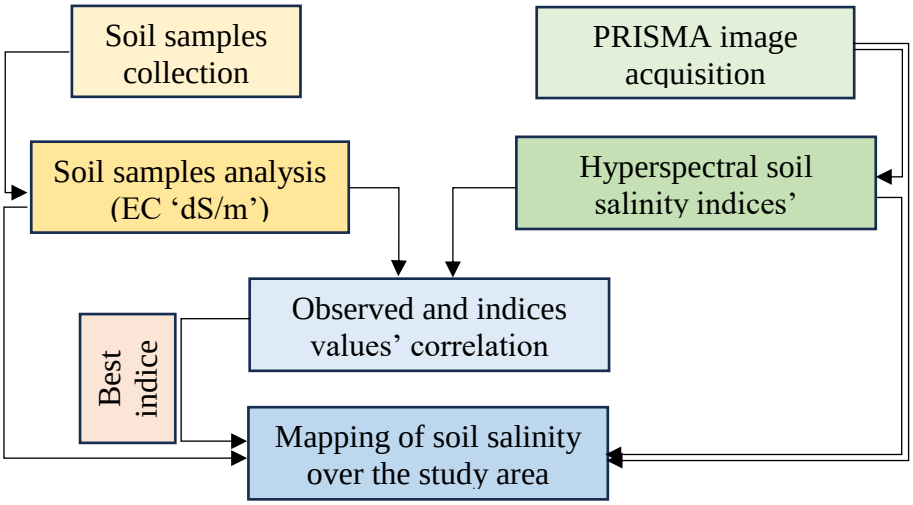

Fig. 1. The materials and methods of the study.

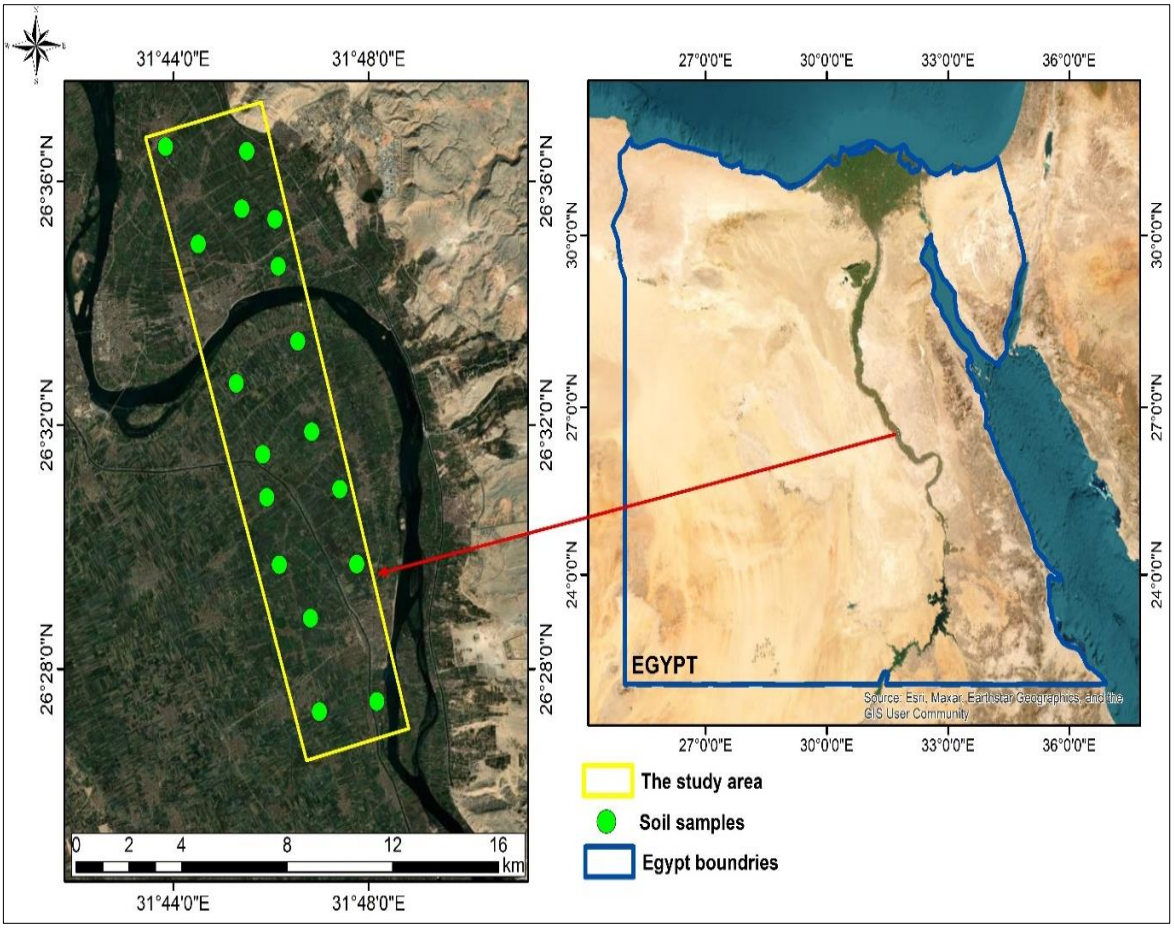

Fig. 2. Location map of the study area with soil profiles.

Figure (4.a) displays the reflectance data of the soil samples' locations. To enhance spectral data quality, prediction accuracy, and soil properties estimating and mapping, hyperspectral noises (bad spectral bands) have been removed (Figure 4.b). The removed spectral bands were from B101 to B122 and from B152 to B182 in SWIR region. The remaining spectral bands, along with laboratory soil property data, were then transferred to an MS Excel spreadsheet for further processing and modeling as shown in Figure (5).

2.5. Hyperspectral variables' selection

The Competitive Adaptive Reweighted Sampling (CARS) algorithm, based on Darwin's "survival of the fittest" principle is used for selecting variables in vis-NIR hyperspectral data, aiming to maximize their correlation with soil properties. Assessing each variable importance is carried out by considering the stability index in CARS model as described in equation (1).

$$\mathbf{C_j} = \left|\frac{\bar{\mathbf{b}}_\mathbf{j}}{\mathbf{S}(\mathbf{b_j})}\right| \qquad (1)$$

The CARS includes four steps as described by Jobson (2012), these steps are; (i) Monte Carlo approach whereas 70% of the dataset are randomly selected to represent the calibration dataset, (ii) during the exponential decreasing function (EDF) stage, the algorithm systematically eliminates less significant variables, as described in equation (2).

$$\boldsymbol{r_i = ae^{-ki}} \qquad (2)$$

whereas the compound $\mathbf{a} = (\frac{\mathbf{P}}{\mathbf{2}})^{\frac{\mathbf{1}}{(\mathbf{N-1})}}$; $\mathbf{k} = \frac{\mathbf{In}\,(\frac{\mathbf{P}}{\mathbf{2}})}{\mathbf{N-1}}$; P = number of total variables; and N is the number of sampling runs, (iii) Adaptive Reweighted Sampling (ARS) that used to competitively eliminate variables after the initial EDF-based elimination, whereas variables having weights exceed a specified threshold are kept, while others are removed, and (iv) quality evaluation of the generated subsets by calculating their respective RMSE values, whereas the lowest subset in RMSE regards is chosen as an optimal.

2.6. The hyperspectral soil salinity indices

The selected hyperspectral bands (12, 23, 31, 33, 43, and 49) derived from the CARS model for soil EC were used to compute various hyperspectral indices. Among these, the COSRI index, as introduced by Fernandez-

Buces et al., (2006), is noteworthy. Vegetation reflectance has proven to be a valuable tool for estimating soil salinity in numerous studies, with many researchers favouring the use of vegetation indices, particularly the NDVI index (Tilley et al., 2007). While NDVI's response to soil salt has been studied, these investigations did not simultaneously consider soil and vegetation. Therefore, Fernandez-Buces et al. (2006) used a modified NDVI to acquire a high correlation with salinity (R^2 >0.8) in a semi-arid Mexican region.
However, this method's predictive power remains untested in other areas, such as arid regions, where NDVI's sensitivity to soil optical properties and limited vegetation information poses challenges.

The COSRI was adapted to predict soil salinity for both bare soil and vegetation areas. Additionally, the NDSI index was described by Khan et al. (2005), the colour index (CI) was described by Huete et al. (1994), the BI index was explained in the studies done by Asfaw et al. (2016) and Dehni and Lounis (2012), and the SI index, incorporating the blue and red band, is particularly responsive to surface reflectance changes in salt-affected, sparsely vegetated areas, demonstrating its ability to effectively differentiate between varying levels of soil salinity (Douaoui et al., 2006). The hyperspectral indices are represented in the following equations (3-8).

$$NDVI = \frac{B43-B33}{B43+B33} \quad (3)$$

$$COSRI = \frac{B12+B23}{B31+B49} * NDVI \quad (4)$$

$$NDSI = \frac{B32-B49}{B32+B49} \quad (5)$$

$$BI = \frac{(B12^2+B23^2+B31^2)}{3} \quad (6)$$

$$CI = \frac{B32-B25}{B32+B25} \quad (7)$$

$$SI = B12 * B31 \quad (8)$$

2.7. Accuracy assessment of each salinity index

After applying each soil salinity index on the PRISMA image, the values of each index which corresponding to the soil profiles' locations were extracted to be correlated with the observed salinity. Regression equations between the observed EC (dS/m) and each soil salinity index were developed based on the correlation coefficient (R^2) and RMSE that were calculated according to the next equations (9-10).

$$\mathrm{RMSE} = \sqrt{\frac{1}{N}\sum_{i=1}^{N}[Z^*(x_i) - Z(x_i)]^2} \quad (9)$$

$$R^2 = N - \left(\frac{\sum(Z^*(x_i)-Z(x_i))^2}{\sum(Y_i-Z(x_i))^2}\right) \quad (10)$$

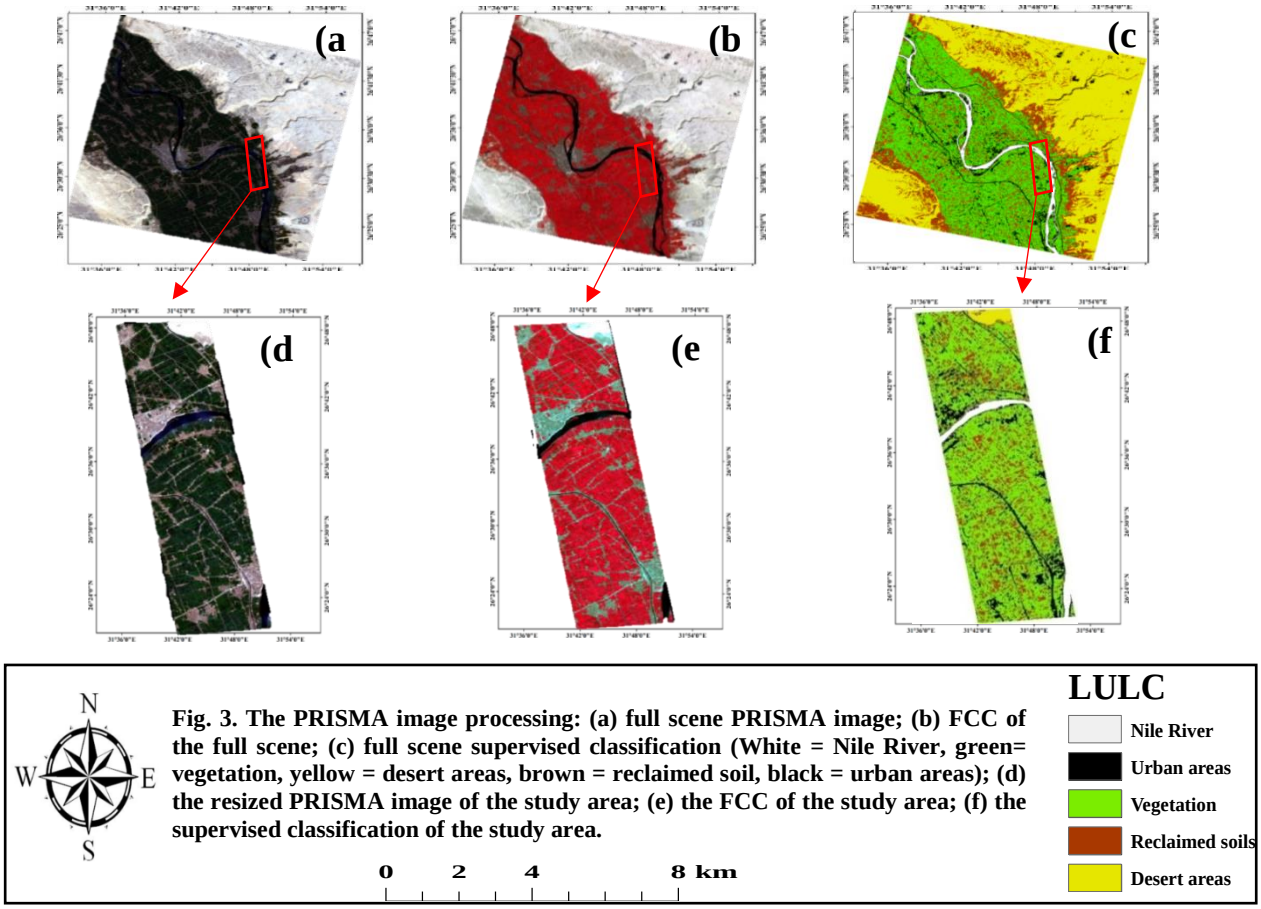

Fig. 3. The PRISMA image processing: (a) full scene PRISMA image; (b) FCC of the full scene; (c) full scene supervised classification (White = Nile River, green= vegetation, yellow = desert areas, brown = reclaimed soil, black = urban areas); (d) the resized PRISMA image of the study area; (e) the FCC of the study area; (f) the supervised classification of the study area.

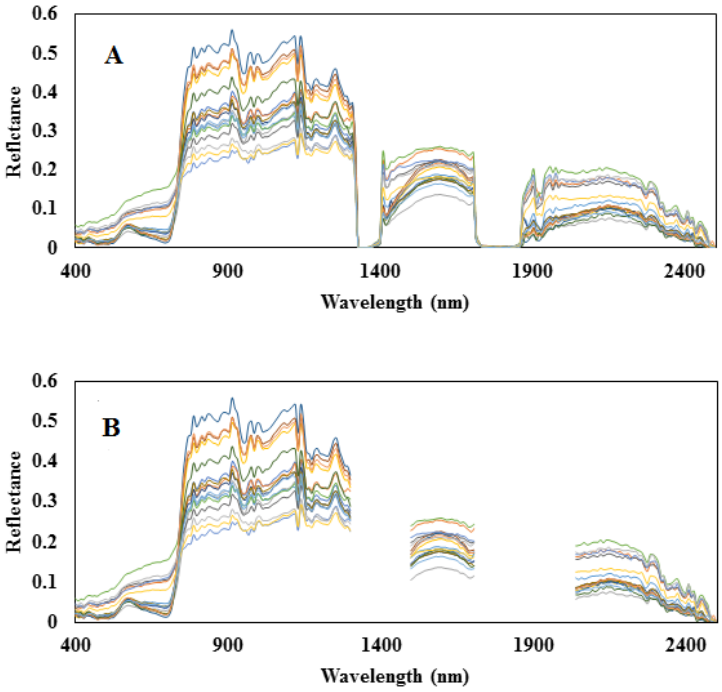

Fig. 4. PRISMA vis-NIR hyperspectral reflectance data of all soil profiles: (a) before removing the spectral noises (bad bands); and (b) after removing spectral noises.

where, RMSE, a widely used metric in evaluating model performance, measures the average difference between predicted salinity values from spectral indices $Z^*(x_i)$ and the actual salinity measurements $Z(x_i)$, indicates the average distance between the data points and the line of best fit with a lower RMSE indicating a tighter clustering of data points N and a higher RMSE suggesting a greater spread. The coefficient of determination (R^2) quantifies how well a regression relation predicts an outcome. R^2 provides insight into how well a linear regression model fits the data. If R^2 is close to 1, the model explains a significant portion of the variance in the dependent variable; whereas if R^2 is close to 0, the model does not explain much of the variance, and the predictions are similar to using the mean of measured values. R^2 represents the proportion of variance in the dependent variable (measured soil salinity) that is explained by the independent variable (s) (predicted value of soil salinity $Z^*(x_i)$.; Ymeas: the mean of the measured values; and $Z(x_i)$ represents the measured value for each data point (x_i).

2.8. Mapping of soil salinity using the hyperspectral indices

Relations between the observed soil EC and the applied hyperspectral salinity indices were established through regression equations. These equations were then applied to PRISMA satellite imagery for mapping the spatial variability of soil EC over the investigated area. This mapping utilized all spectral soil salinity indices and was conducted using ENVI 5.3 software.

3. Results

3.1.Soil Properties

As data given in Table 1, the soil pH values of the investigated area differ between 7.71 and 8.13. These soils are considered as slightly alkaline, moderately alkaline according to **Schoenberger et al. (2012)**. The soil salinity data (EC_e dS/m), was analyzed to understand its distribution within the soil profiles. The data exhibited a moderate range of 1.20 dS/m, with a minimum of 0.85 dS/m, maximum of 2.10 dS/m. According to the classification of soil salinity suggested by **Schoenberger et al. (2012)**, approximately 94.12 % of the total soil profiles are non-saline (ECe <2 dS/m), while 5.88 % of them are very slightly saline (EC_e 2 to <4 dS/m) as shown in Table 1. Concerning the calcium carbonate content of the studied soil peofiles varies from 0.65 to 3.71%. The soil profiles in the studied area are slightly calcareous according to the classification which prepared by **Schoenberger et al. (2012).** Regarding The bicarbonate ions (HCO_3^-) in the saturated soil past extract of the studied soil profiles differ from 2.30 to 6.15 meq/L (Table 1). Meanwhile, chloride ion (Cl^-) concentrations of

the studied soil profiles extend from 3.38 to 7.34 meq/L. The soluble sulfate (SO_4^{-2}) of the studied soils varies from 0.25 to 3.08 meq/L. Generally, the soluble anions in the saturated soil paste extract of these soils could be arranged in the descending order of $Cl^- > HCO_3^- > SO_4^{-2}$. The obtained results reveal that the soluble calcium ions (Ca^{+2}) range between 1.99 and 6.64 meq/L. Moreover, the soluble magnesium (Mg^{+2}) concentration is generally less than the soluble calcium in the investigated soil profiles that differs from 1.01 to 4.22 meq/L. The findings also observed that the soluble sodium (Na^+) in the studied soils varies between 3.08 and 6.47 meq/L.Whlist the soluble potassium ion (K^+) concentrations of the investigated soil profiles range from 0.26 to 2.09 meq/L (Table 1). Generally, the soluble cations in the saturated soil paste extract of these soils could be ranked in the decreasing order of $Na^+ > Ca^{+2} > Mg^{+2} > K^+$. In regard to the sodium adsorption ratio (SAR_e) of the soil profiles differ among 1.87 to 3.67. According to **Bohn et al. (2001)**, these soils have a SAR_e value of less than 13 which they are considered non-sodic soils. As data given in Table 1, the CEC values of the studied soil profiles vary from 19.44 to 23.58 cmol (+)/kg. Figure (5) visually depicts the spatial distribution of soil salinity (EC values) across the study area, highlighting areas with high and low salinity levels.

3.2.The derived soil spectral salinity indices

The applied indices (NDVI; COSRI; NDSI; CI; BI; and SI) were mapped to display the spatial variability of the soil salinity over the investigated area, as presented in the Figure (6). The NDVI index which is a relation between the red and near infrared (NIR) classified the soil surface to several classes based on the soil cover. Moreover, when the vegetation cover increase, the bare soil decrease, and soil salinity decrease. Furthermore, the reflectance of other surface objects such as water bodies represented as high salinity because NDVI is a relation of soil and vegetation. Figure (7) showed this relation between NDVI and salinity. The typical relation was observed for COSRI whereas a positive correlation between NDVI and COSRI. The more NDVI, the more COSRI, and the low salinity. The NDSI is typically similar to the NDVI in the values range (-1 to 1); while the NDSI used for identifying the soil salinity in the land surface using the green and shortwave infra-red (SWIR) spectral bands. The BI works in the visible-near-infra-red (Vis-NIR) range of spectra. It plays a crucial role in soil salinity mapping which it can analyse the brightness variations in the soil surface. Moreover, BI helps identify areas with higher salt content. The CI assesses soil colour variations, indirectly providing insights into soil composition and salinity. Meanwhile, the SI specifically targets soil salinity assessment, considering factors like EC. SI aids in evaluating soil salinity severity, impacting plant growth and land use decisions.

Table 1. Profiles weighted mean of some soil characteristics of the studied area.

Profile No	pH	EC_e dS/m	$CaCO_3$ %	Soluble anions (meq/L)			Soluble cations (meq/L)				SAR_e	CEC cmol(+)/kg
				HCO_3^{-1}	Cl^{-1}	SO_4^{-2}	Ca^{+2}	Mg^{+2}	Na^{+1}	K^{+1}		
1	7.77	1.11	3.52	2.3	5.72	1.01	3.08	2.48	4.46	0.49	2.68	20.91
2	8.02	1.08	3.11	3.53	6.34	0.68	3.41	2.21	3.9	0.79	2.33	19.44
3	7.89	0.85	1.26	4.07	3.49	0.25	1.99	1.01	4.5	0.71	3.67	20.29
4	8.01	0.93	2.5	3.89	4	0.47	3.86	1.73	3.15	0.26	1.88	21.23
5	7.93	0.93	2.45	4.21	4.39	0.29	3.68	1.35	3.08	0.34	1.94	20.79
6	7.86	0.86	2	3.6	4.03	0.61	3.23	1.16	3.41	0.41	2.3	20.48
7	7.79	1.27	2.88	3.53	5.9	1.58	4.91	1.58	4.16	0.86	2.31	21.82
8	7.73	0.94	1.57	4.75	3.49	0.61	4.09	1.35	3.71	0.34	2.25	19.83
9	7.98	1.2	0.65	4	4.18	1.15	3.53	2.06	4.05	0.45	2.42	19.99
10	8.07	1.08	3.71	4.64	4.03	0.65	4.2	2.18	3.34	0.79	1.87	22.45
11	7.96	1.11	3.21	4.64	5.62	0.86	3.68	1.39	4.58	1.09	2.88	20.14
12	7.71	0.98	2.46	3.49	3.38	1.12	4.99	2.93	3.75	1.05	1.89	21.07
13	7.72	1.23	2.11	5.26	5.26	0.61	4.73	2.1	4.13	0.64	2.23	20.91
14	7.99	1.16	1.16	4.07	4.43	1.58	4.43	1.8	4.09	0.83	2.32	20.94
15	8.13	2.1	1	6.15	7.34	3.08	6.64	4.22	6.47	2.09	2.78	21.08
16	7.94	0.89	1.24	3.2	4.75	0.25	3.34	1.28	3.64	0.49	2.4	23.58
17	8.03	1.01	1.13	3.85	3.71	1.19	3	1.46	4.61	0.38	3.09	21.63

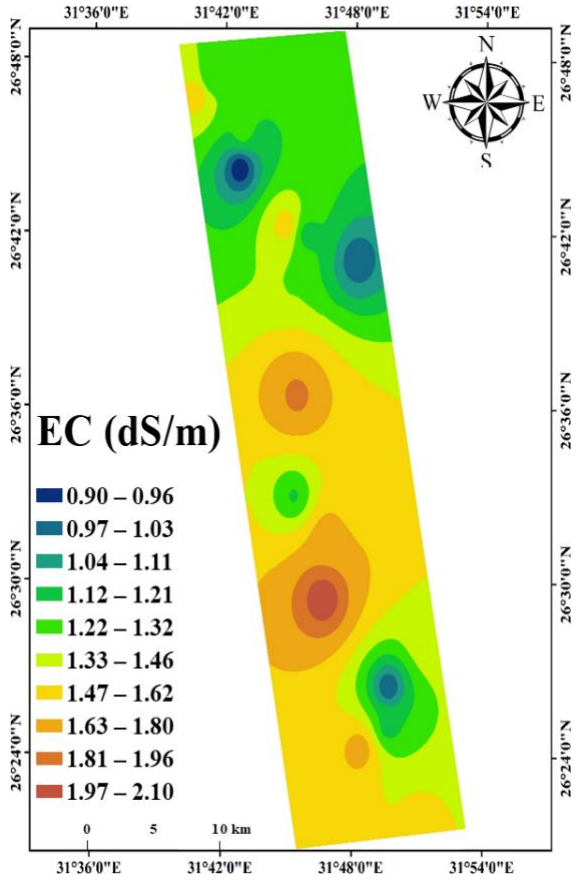

Fig. 5. The spatial variability map of soil salinity (EC 'dS/m') of the study area.

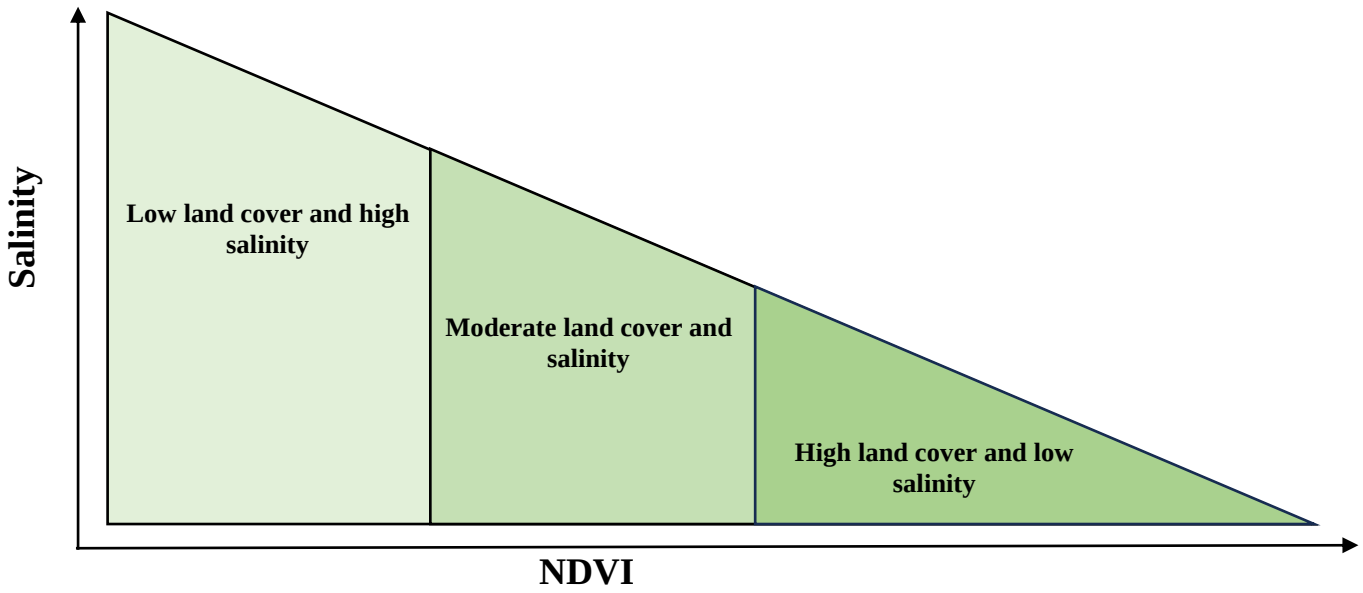

Fig. 6. Relation of NDVI and salinity.

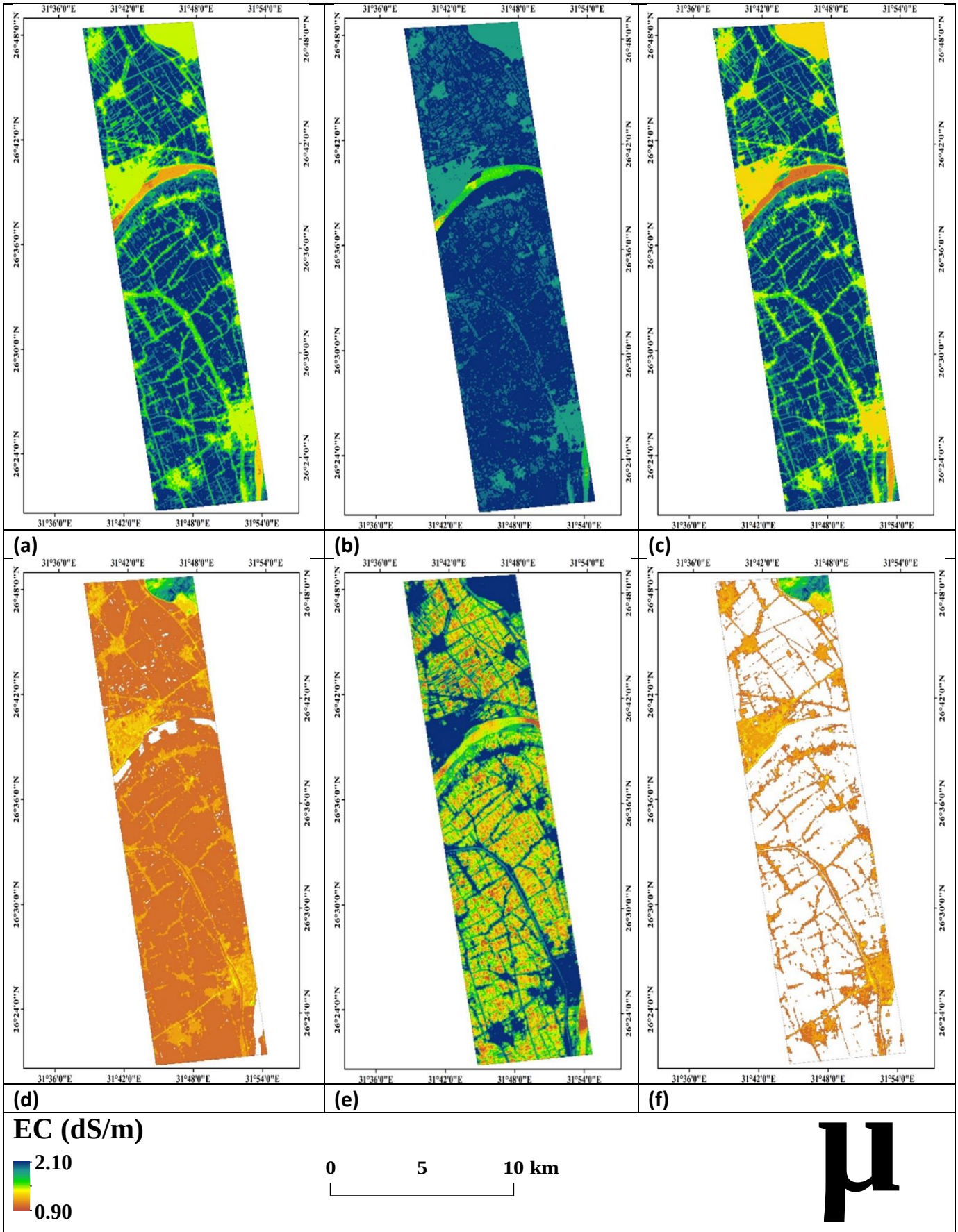

Fig. 7. Spatial variability maps of spectral soil salinity indices: (a) NDVI; (b) COSRI; (c) NDSI; (d) CI; (e) BI; and (f) SI.

3.3.Accuracy assessment of the applied indices

Table (2) demonstrated the accuracy of each index in mapping soil salinity, assessed using R^2, RMSE and regression equations. The obtained data revealed that the best index for mapping soil salinity was COSRI which had R^2 value of 0.6781 and RMSE of 0.267 dS/m. The second-best index was CI whereas R^2 and RMSE values were 0.6376 and 0.297 dS/m, respectively. The NDVI showed moderate performance in mapping soil salinity which recorded R^2 of 0.5269 and RMSE of 0.127 dS/m. Moreover, the NDSI achieved the same performance of NDVI with R^2 and RMSE values of 0.5098 and 0.267 dS/m, respectively. Furthermore, the CI model achieved similar accuracy for mapping soil salinity with R^2 of 0.5304 and RMSE of 0.297 dS/m. The lowest accuracy was recorded for the SI (R^2 = 0.1129 and RMSE = 0.326 dS/m). Figure (8) showed the scatter plotting between the observed or measured values of the EC (dS/m) and the predicted soil salinity values using derived indices.

4. Discussion

4.1. Soil salinity in the study area

The soil salinity of the study area was low is similar to the average soil salinity levels in the other regions (Moustafa (2023); Thabit et al. (2023); and Moursy and Thabit (2022)). Low salinity soils offer several advantages for plant growth and crop production. These include improved plant growth due to better water accessibility, higher crop yields, reduced drought stress, easier nutrient uptake, and prevention of desertification (Mustafa and Akhtar 2019; Ganzour et al., 2024) Proper management is essential to maximize these benefits. Sohag soil have been mapped for their salinity by many research studies. Among them, Moustafa and Moursy (2020) utilized the analytical hierarchy process (AHP) and GIS approaches for mapping some soil properties of some soils in Sohag included the soil salinity. Ismail et al. (2024) utilized the remote sensing and GIS tools for mapping several soil types as well as some physicochemical soil properties in Elbahrya Oasis region. Soil salinity can arise from natural or anthropogenic factors. Primary salinization as a natural process occurs primarily due to the presence of soluble salts in the soil, including sodium, calcium, and magnesium, these salts originate from the weathering of rocks and minerals and can be transported to the soil surface through various natural processes. The physical or chemical weathering is another process whereas the breakdown of minerals releases salts into the soil (Zaman et al., 2018). The anthropogenic factors which are considered as secondary salinization include the overuse of irrigation water which can lead to salt accumulation in the soil. Climate change also affect soil salinity; while intensive farming practices can also exacerbate salinization. Another important reason is Poor Drainage or Waterlogging whereas, inadequate water transport prevents salt removal from the soil. Certainly, evaporation concentrates salts at the surface (Stavi et al., 2021). There are many processes which can be followed in order to mitigate the impacts of soils salinity. Among these processes, improving the irrigation practices (Saffan et al., 2024). Farmers can explore using brackish water for irrigation to reduce reliance on saline river water. Moreover, precise application of water minimizes salt accumulation. Promoting crops adapted to saline conditions can mitigate yield losses. Furthermore, constructing and maintaining efficient drainage networks is crucial. Besides, installing subsurface drains helps remove excess salts. Traditional methods for determining soil salinity have drawbacks, including being time-consuming, operator-dependent, labour-intensive, limited in spatial coverage, inadequate for dynamic environments, and costly. Modern techniques, such as satellite imagery and remote sensing, offer more efficient and comprehensive ways to monitor soil salinity.

4.2. Hyperspectral remote sensing for soil salinity estimation

Hyperspectral remote sensing technology provides several advantages for estimating soil salinity. First, it offers high-resolution data with continuous spectral bands, allowing precise discrimination of soil properties (Chen et al., 2023). Second, it enables dynamic monitoring by collecting data repeatedly over time, aiding in real-time decision-making. Third, it is non-destructive and rapid, suitable for large-scale surveys (Shaik et al., 2023). Finally, hyperspectral bands are sensitive to soil characteristics, including salinity, facilitating accurate retrieval of salinity data (Chen et al., 2023). Earlier research has investigated the possibilities of utilizing PRISMA hyperspectral remote sensing to evaluate soil salinity. However, a thorough review emphasized the difficulties associated with using remote sensing tools for estimating soil salinity on a large scale. These challenges primarily stem from limitations in data resolution and the high costs involved in data acquisition.

Table 2. The accuracy assessment and repression equations of all spectral soil salinity indices.

Index	R^2	RMSE (dS/m)	Regression equation
NDVI	0.5269	0.127	y = 0.2356*NDVI + 1.2554
COSRI	0.6781	0.267	y = 6.3984*COSRI + 0.6249
NDSI	0.5098	0.489	y = -0.2246*NDSI + 1.2468
CI	0.6376	0.297	y = -26.167*CI + 1.4501
BI	0.5304	0.297	y = 113.75*BI + 0.918
SI	0.1128	0.326	y = -0.3219*SI + 1.3694

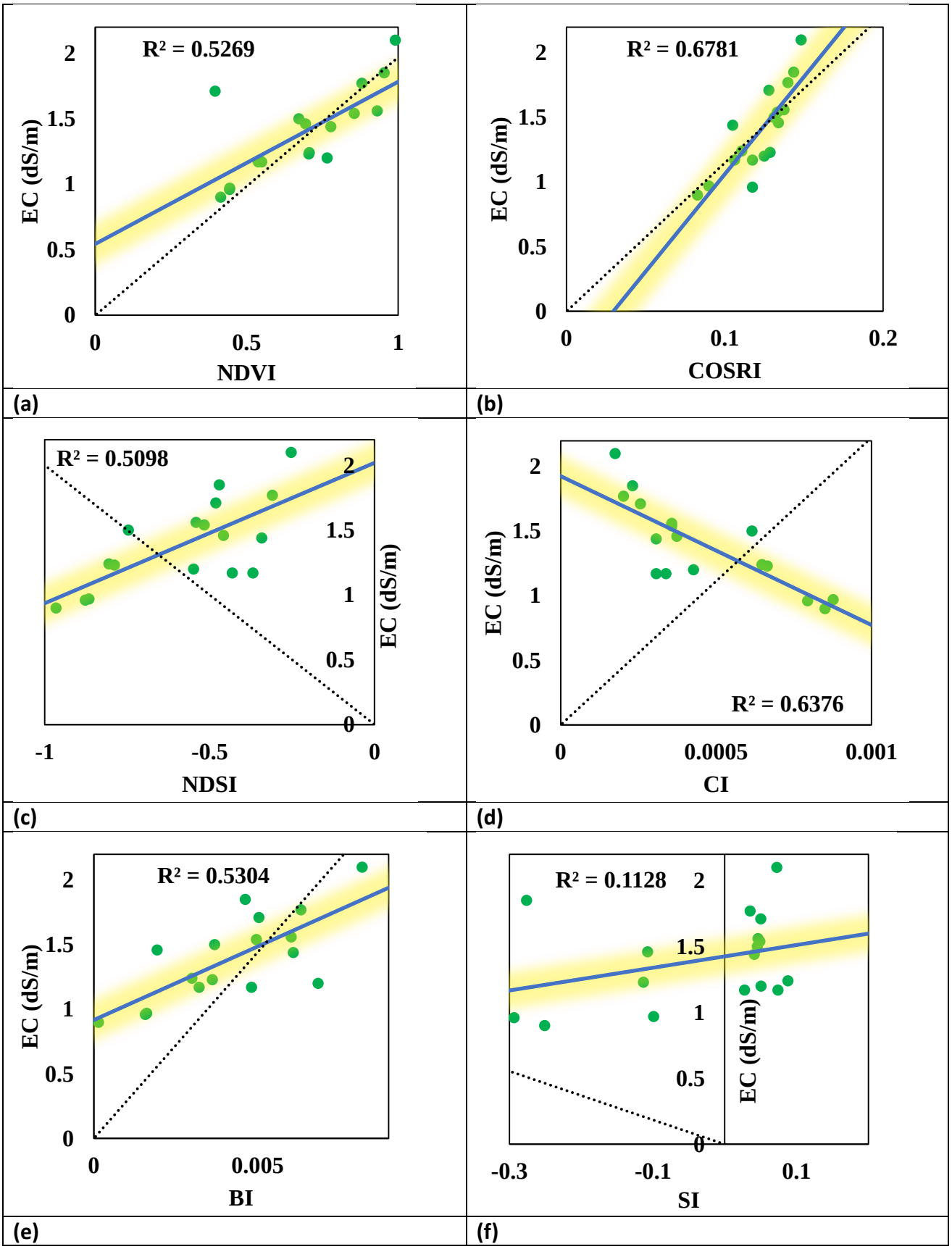

Fig. 8. Scatter plots between the measured EC (dS/m) and: (a) NDVI; (b) COSRI; (c) NDSI; (d) CI; (e) BI; and (f) SI.

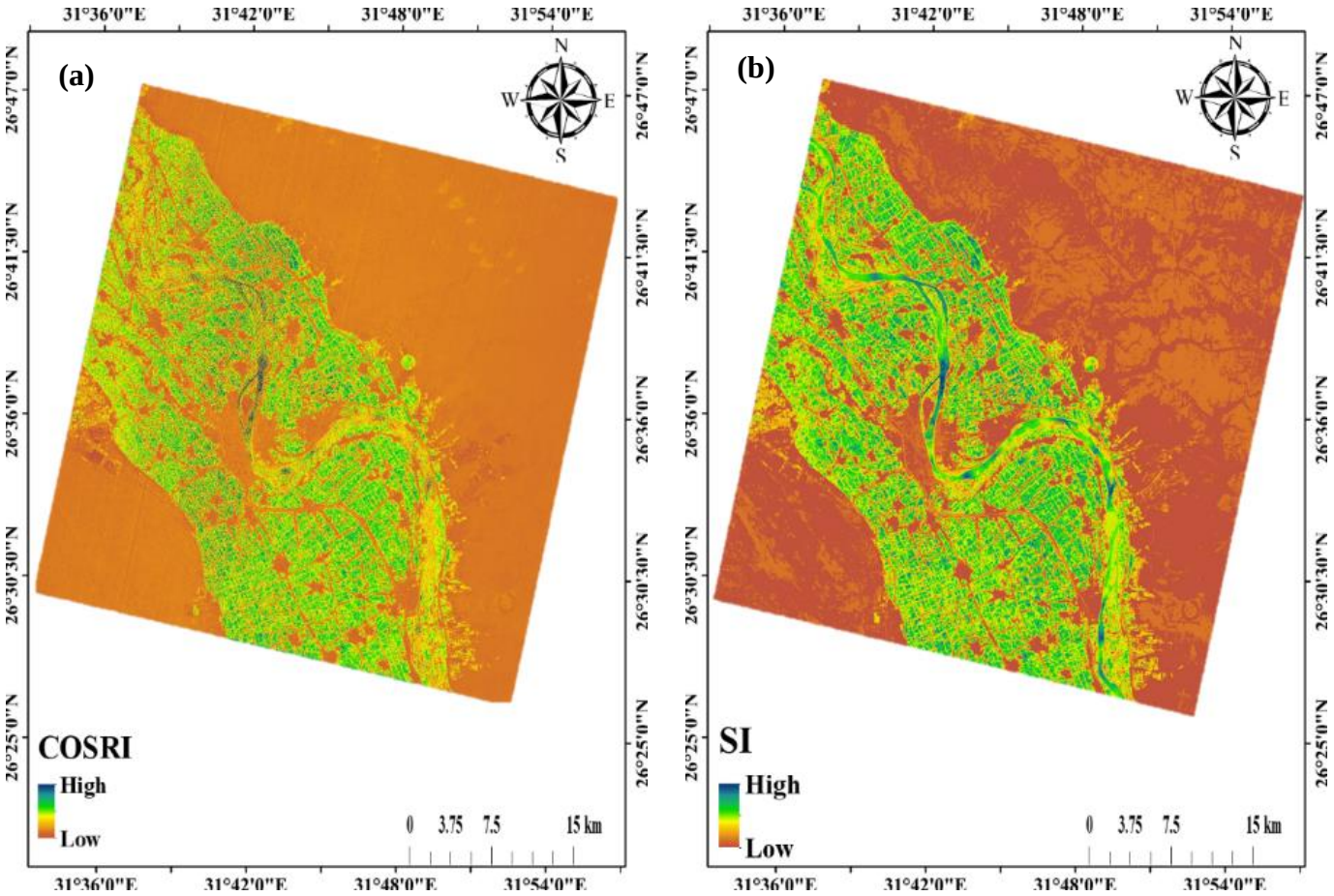

Fig. 9. Spatial variability maps of soil salinity using the best spectral salinity indices: (a) COSRI; and (b) SI.

In summary, the review underscored the ongoing challenges faced in employing remote sensing for widespread assessment of soil salinity due to resolution and cost constraints (Sahbeni et al., 2023). In practical salinization mapping, achieving a balance between data resolution, spatial and temporal coverage, acquisition costs, and high accuracy expectations often involves making trade-offs. Another article discussed the role of the hyperspectral remote sensing data especially PRISMA images in estimating soil salinity (Cala et al., 2022).

4.3. Spectral salinity indices

Hyperspectral salinity indices such as COSRI and SI have proven a good efficiency for soil salinity mapping, however, similar findings were achieved by Ma and Tashpolat (2023). They recorded R^2 value of above 0.60 when regretted with the soil EC observed values. El-Horiny (2019) mapped the soil EC in the Bahariya Oasis, Western Desert of Egypt using the SI (R^2 = >0.80). Han et al. (2023) conducted a study in Da'an City, utilizing machine learning techniques and Landsat 8 OLI imagery to estimate soil salinity. They calculated a comprehensive set of 19 spectral indexes, encompassing 15 salinity indexes, 3 vegetation indexes, and a brightness index, utilizing the blue, green, red, and near-infrared bands of Landsat 8 OLI images. Notably, their study found the Cubist model to exhibit the highest prediction accuracy (RMSE=0.31 mS/cm), with the canopy salinity index (CRSI) displaying the strongest correlation with measured electrical conductivity (correlation coefficient of −0.44). Based on their findings, the Cubist method is recommended for soil salinity monitoring in arid and semi-arid regions. In India, Kumar et al. (2015) utilized hyperspectral remote sensing data to derive spectral indices for characterizing salt-affected soils. Among these indices, the SI index exhibited strong correlations with salinity-related parameters, including EC value (R^2 = 0.81), pH (R^2 = 0.51), exchangeable sodium percentage (ESP) (R^2 = 0.80), and sodium adsorption ratio (SAR) (R^2 = 0.80).

Additionally, the BI index also showed significant correlations with soil properties, such as EC (R^2 = 0.77), pH (R^2 = 0.49), EC (R^2 = 0.73), ESP (R^2 = 0.79), and SAR (R^2 = 0.77). These two spectral indices; SI and BI are

particularly useful for mapping salt-affected soil parameters. Notably, they rely on spectral bands at wavelengths 9, 20, and 28, which represent shorter regions of the electromagnetic spectrum. In contrast, the NDSI index, based on NIR wavelengths (813.48 nm, corresponding to band 46), demonstrated weaker correlations with soil salinity compared to SI, BI, and COSRI spectral indices. Similarly, Fernández-Buces et al. (2006) also highlighted the strong correlation between COSRI and BI and soil salinity. In a study by Liu et al. (2018), they found that the NDVI index exhibits minimal correlation with soil salinity, whether at a depth of 10 cm or 4 cm. Interestingly, the correlation at the 4 cm depth is slightly higher ($R^2 = 0.042$) compared to the 10 cm depth ($R^2 = 0.032$). It is hardly to find any research study used the PRISMA hyperspectral imageries for assessing the soil salinity.

5. Conclusion

The utilization of PRISMA visible-Near-Infrared (vis-NIR) hyperspectral images has demonstrated promise in estimating and mapping soil salinity within a specific region of Sohag, Egypt. In this study, seventeen representative soil profiles were meticulously collected and analyzed for their EC/dS/m values. Additionally, the PRISMA hyperspectral image of the study area was acquired, processed, and several soil salinity hyperspectral indices were applied, including SI, BI, NDSI, COSRI, and CI indices.

Among the spectral bands captured by the PRISMA image, six specific bands (Band 12, 23, 25, 31, 32, and 49) were deemed significant and utilized for calculating the hyperspectral indices. Spatial variability maps of soil salinity were generated by establishing a relationship between these developed hyperspectral indices and observed soil salinity (EC dS/m).

The results revealed that soil EC in the study area ranged from 0.9 to 2.10 dS/m, with a mean value of 1.40 dS/m. Interestingly, the generated maps indicated a relatively small range of salinity across the study area. Notably, the COSRI and CI hyperspectral salinity indices exhibited superior performance in estimating soil salinity (EC). Specifically, the R^2 values for these indices were 0.6781 and 0.6376, respectively, while the RMSE values were 0.267 and 0.297 dS/m, respectively.

In contrast, other indices such as; NDVI, NDSI, BI, and SI demonstrated lower capability for estimating soil salinity over the investigated area. Overall, the PRISMA hyperspectral data holds significant potential for enhancing land management practices by accurately estimating soil salinity in the specified part of Sohag, Egypt.

Declarations

Ethics approval and consent to participate

Consent for publication: The article contains no such material that may be unlawful, defamatory, or which would, if published, in any way whatsoever, violate the terms and conditions as laid down in the agreement.

Availability of data and material: Not applicable.

Competing interests: The authors declare that they have no conflict of interest in the publication.

Funding: Not applicable.

Authors' contributions: Authors A.R.A.M., M.A.E., M.E.F., and A.H.A.; methodology, A.R.A.M, M.A.E., M.E.F., and A.H.A.; software, A.R.A.M, M.A.E., M.E.F., and A.H.A.; formal analysis, A.R.A.M, M.A.E., M.E.F., and A.H.A.; investigation, A.R.A.M, M.A.E., M.E.F., and A.H.A.; writing—original draft preparation, A.R.A.M , M.A.E., M.E.F., and A.H.A.; writing review and editing and finalize the manuscript. All authors read and agree to submit their manuscripts to the journal..

References

Abd El-Aziz, S. H., Gameh, M. A., and Ghallab, A. (2018). Applications of geographic information systems in studying changes in groundwater quality and soil salinity in Sohag Governorate. Eurasian Journal of Soil Science, 7(3), 213-223.

Abdel-rahman, A. M., and Negim, O. E. (2016). Utilizing of geoinformatics for mapping land use/land cover changes in Sohag, Egypt. American Journal of Environmental Engineering and Science, 3(1), 33-42.

Alvarenga, P., P. Palma, A. de Varennes and A.C. Cunha-Queda. (2012). A contribution towards the risk assessment of soils from the São Domingos Mine (Portugal): Chemical, microbial and ecotoxicological indicators, Environ. Pollut., 161: 50-56.

Asfaw, E., Suryabhagavan, K.V., Argaw, M. (2016). Soil salinity modeling and mapping using remote sensing and GIS: The case of Wonji sugar cane irrigation farm, Ethiopia. Journal of the Saudi Society of Agricultural Sciences.

Barrow, N.J. (1993). Mechanisms of Reaction of Zinc with Soil and Soil Components. In: Robson, A.D. (eds) Zinc in Soils and Plants. Developments in Plant and Soil Sciences, vol 55. Springer, Dordrecht. https://doi.org/10.1007/978-94-011-0878-2_2

Bashour, I. and A. Sayegh. (2007). Methods of Analysis for Soil in Arid and Semi-Arid Regions FAO, Roma, p 119.

Bohn, H.L., B.L. McNeal and G.A. O'Connor. 2001. Soil Chemistry. 3rd edition. JohnWiley & Sons, Inc. New York., USA.

Cala, A., Maturana-Cordoba, A., and Soto-Verjel, J. (2023). Exploring the pretreatments' influence on pressure reverse osmosis: PRISMA review. Renewable and Sustainable Energy Reviews, 188, 113866.

Cao, Q., Yu, G., and Qiao, Z. (2023). Application and recent progress of inland water monitoring using remote sensing techniques. Environmental Monitoring and Assessment, 195(1), 125.

Chen, B., Liu, L., Zou, Z., and Shi, Z. (2023). Target Detection in Hyperspectral Remote Sensing Image: Current Status and Challenges. Remote Sensing, 15(13), 3223.

Dehni A., Lounis M.(2012). Remote sensing techniques for salt affected soil mapping: Application to the Oran region of Algeria. In Procedia Engineering. 33, 188.

El-Aziz, A., Hassanien, S., Ibrahim, A. G. M., Mohamed, E. G., El-Azem, A., & Alaa, H. (2024). Characterization of The Spatial Variability of Some Soil Physicochemical Properties of The El-Gallaba Plain, New Aswan City, Aswan Governorate, Egypt. Egyptian Journal of Soil Science, 64(1), 153-166.

Essa, M.A., & Farragallah, M.E.A. (2020). Clay minerals and their interactions with heavy metals and microbes of soils irrigated by various water resources at Assiut, Egypt. AUCES, 1(1), 73-87. Retrieved from https://auber.journals.ekb.eg/article_150282_f59b8cf9fc1b3703dbde662a388851af.pdf

Ewing, J., Oommen, T., Jayakumar, P., Alger, R. (2020). Utilizing Hyperspectral Remote Sensing for Soil Gradation. *Remote Sensing*. 12(20):3312. https://doi.org/10.3390/rs12203312.

El-Horiny, M. M. (2019, July). Mapping and monitoring of soil salinization using remote sensing and regression techniques: A case study in the Bahariya depression, Western Desert, Egypt. In IGARSS 2019-2019 IEEE International Geoscience and Remote Sensing Symposium (pp. 1-4). IEEE.

Fadl, Mohamed E., Mohamed E. M. Jalhoum, Mohamed A. E. AbdelRahman, Elsherbiny A. Ali, Wessam R. Zahra, Ahmed S. Abuzaid, Costanza Fiorentino, Paola D'Antonio, Abdelaziz A. Belal, and Antonio Scopa. (2023). "Soil Salinity Assessing and Mapping Using Several Statistical and Distribution Techniques in Arid and Semi-Arid Ecosystems, Egypt" *Agronomy* 13, no. 2: 583. https://doi.org/10.3390/agronomy13020583

Fernandez-Buces, N., Siebe, C., Cram, S., and Palacio, J. L. (2006). Mapping soil salinity using a combined spectral response index for bare soil and vegetation: A case study in the former lake Texcoco, Mexico. Journal of Arid Environments, 65(4), 644-667.

Ganzour, S. K., Aboukota, M. E. S., Hassaballa, H., & Elhini, M. (2024). Land Degradation, Desertification & Environmental Sensitivity to Climate Change in Alexandria and Beheira, Egypt. Egyptian Journal of Soil Science, 64(1).

Gorji, T., Sertel, E., and Tanik, A. (2017). Recent satellite technologies for soil salinity assessment with special focus on Mediterranean countries. Fresenius Environ. Bull, 26(1), 196-203.

Hamzeh, S., Naseri, A. A., AlaviPanah, S. K., Bartholomeus, H., and Herold, M. (2016). Assessing the accuracy of hyperspectral and multispectral satellite imagery for categorical and quantitative mapping of salinity stress in sugarcane fields. International journal of applied earth observation and geoinformation, 52, 412-421.

Han, Y., Ge, H., Xu, Y., Zhuang, L., Wang, F., Gu, Q., and Li, X. (2023). Estimating soil salinity using multiple spectral indexes and machine learning algorithm in songnen plain, China. IEEE Journal of Selected Topics in Applied Earth Observations and Remote Sensing, 16, 7041-7050.

Hassani, A., Azapagic, A., and N. Shokri, (2020). "Predicting long-term dynamics of soil salinity and sodicity on a global scale," Proc. Nat. Acad. Sci., vol. 117, no. 52, pp. 33017–33027, Dec..

Hu, J., Peng, J., Zhou, Y., Xu, D., Zhao, R., Jiang, Q., and Shi, Z. (2019). Quantitative estimation of soil salinity using UAV-borne hyperspectral and satellite multispectral images. Remote Sensing, 11(7), 736.

Huete, A. R., Liu, H., de Lira, G. R.,(1994). A soil color index to adjust for soil and litter noise in vegetation index imagery of arid regions. Geoscience and Remote Sensing Symposium, 2: 1042-1043.

Ibrahim, M. S., Hassan, M., and Osman, H. (2021). The cultivation period effects on heavy metals content of some soils of Sohag governorate. Journal of Sohag Agriscience (JSAS), 6(2), 124-136.

Ismail, M. S., Ghonamey, E., Kotb, Y., Ganzour, S. K., & Allam, A. S. (2024). Mapping Soil Types in the North El Bahrya Oases, Egypt, using Remote Sensing and GIS for Agricultural Planning. Egyptian Journal of Soil Science, 64(4), 1315-1338.

Jackson, M.L. (1973). Soil chemical analysis.Prentice-Hall of India Private limited, New Delhi, p 498.

Jalali, J., Ahmadi, A., and Abbaspour, K., (2021). Runoff responses to human activities and climate change in an arid watershed of central Iran, Hydrological Sci. J., vol. 66, no. 16, pp. 2280–2297.

Kumar, S., Gautam, G., and Saha, S. K. (2015). Hyperspectral remote sensing data derived spectral indices in characterizing salt-affected soils: a case study of Indo-Gangetic plains of India. Environmental Earth Sciences, 73, 3299-3308.

Lassalle, G., Ferreira, M. P., La Rosa, L. E. C., Scafutto, R. D. P. M., and de Souza Filho, C. R. (2023). Advances in multi- and hyperspectral remote sensing of mangrove species: A synthesis and study case on airborne and multisource spaceborne imagery. ISPRS Journal of Photogrammetry and Remote Sensing, 195, 298-312.

Liu, L., Ji, M., and Buchroithner, M. (2018). A case study of the forced invariance approach for soil salinity estimation in vegetation-covered terrain using airborne hyperspectral imagery. ISPRS international journal of geo-information, 7(2), 48.

M. Zaman, S. A. Shahid, and L. Heng, Guideline for Salinity Assessment, Mitigation and Adaptation Using Nuclear and Related Techniques. Cham, Switzerland: Springer, 2018.

Ma, Y., and Tashpolat, N. (2023). Remote Sensing Monitoring of Soil Salinity in Weigan River–Kuqa River Delta Oasis Based on Two-Dimensional Feature Space. Water, 15(9), 1694.

Moursy, A. R., and Thabit, F. N. (2022). Soil Characterization and Estimation of the Current and Future Productivity of the Faculty of Agriculture Farm, Sohag University, Egypt. Journal of Soil Sciences and Agricultural Engineering, 13(9), 295-302.

Mustafa, A. A. (2023). Incorporate the Fertility Capability Classification and Geo-informatics for Assessing Soil: A Case Study on Some Soils of Sohag Governorate, Egypt. Journal of Soil Sciences and Agricultural Engineering, 14(7), 187-193.

Mustafa, A. E. R. A., and Moursy, A. R. (2020). Integration of geoinformatics and AHP model for soil site suitability analysis for the major crops in Sohag, Egypt. International Journal of Recent Advances in Multidisciplinary Research, 7(7), 5784-5796.

Mustafa, G., and Akhtar, M. S. (2019). Crops and methods to control soil salinity. Salt Stress, Microbes, and Plant Interactions: Mechanisms and Molecular Approaches: Volume 2, 237-251.

Negim, O. I., and Moursy, A. R. A. (2023). Effect of Long-Term Irrigation with Sewage Wastewater on Land Capability of Three Sites in Sohag Governorate, Egypt. Journal of Soil Sciences and Agricultural Engineering, 14(8), 235-246.

Nelson, R.E. (1982). Carbonate and gypsum. P. 181-198. In A. L. Page, R.H. Miller and D.R. Keeney (eds.) Methods of soil analysis. Part 2- Chemical and microbiological properties (2nd edition). Agronomy 9: Am. Soil Sci. Soc., Madison, WI., USA.

Ghanbari, R., Heidarimozaffar, M., Soltani, A., and Arefi, H. (2023). Land surface temperature analysis in densely populated zones from the perspective of spectral indices and urban morphology, Int. J. Environ. Sci. Technol., vol. 20, no. 3, pp. 2883–2902.

Rafie, R. (2024). Effect of Water Table on Soil and Wheat Productivity in Siwa Oasis. Egyptian Journal of Soil Science 64(4).

Richards, L.A. (1954). Diagnosis and Improvement of Saline and alkali Soils.United States Salinity Laboratory Staff, Department of Agriculture, Hand Book, No.60.California, USA.

Sahbeni, G., Ngabire, M., Musyimi, P. K., and Székely, B. (2023). Challenges and opportunities in remote sensing for soil salinization mapping and monitoring: A review. Remote Sensing, 15(10), 2540.

Saffan, M. M., El-Henawy, A. S., Agezo, N. A., & Elmahdy, S. (2024). Effect of irrigation water quality on chemical and physical properties of soils. Egyptian Journal of Soil Science, 64(4).

Schoenberger, P.J., D.A. Wysocki, E.C. Benham and Soil Survey Staff. (2012). Field Book for Describing and Sampling Soils, Version 3.0. Natural Resources Conservation Service, National Soil Survey Center, Lincoln, NE.

Seifollahi-Aghmiuni, S., Kalantari, Z., Egidi, G., Gaburova, L., Salvati, L. (2022). Urbanisation-driven land degradation and socioeconomic challenges in peri-urban areas: Insights from Southern Europe. Ambio. 2022 Jun;51(6):1446-1458. doi: 10.1007/s13280-022-01701-7. PMID: 35094245; PMCID: PMC9005568.

Shaik, R. U., Periasamy, S., and Zeng, W. (2023). Potential assessment of PRISMA hyperspectral imagery for remote sensing applications. Remote Sensing, 15(5), 1378.

Shen, L., Gao, M., Yan, J., Li, Z-L., Leng, P., Yang, Q., Duan, S-B. (2020). Hyperspectral Estimation of Soil Organic Matter Content using Different Spectral Preprocessing Techniques and PLSR Method. *Remote Sensing*. 12(7):1206. https://doi.org/10.3390/rs12071206.

Shepherd, K. D. and Walsh, M. G.(2002). Development of reflectance spectral libraries for characterization of soil properties Soil Sci. Soc. Amer. J., vol. 66, no. 3, pp. 988–998,.

Stavi, I., Thevs, N., and Priori, S. (2021). Soil salinity and sodicity in drylands: A review of causes, effects, monitoring, and restoration measures. Frontiers in Environmental Science, 9, 712831.

Trehan, S.P., & Sekhon, G.S. (1977). Effect of clay, organic matter and CaCO3 content on zinc adsorption by soils. Plant Soil, 46(2), 329–336. https://doi.org/10.1007/BF00010089

Thabit, F. N., Negim, O. I., Abdelrahman, M. A., Scopa, A., and Moursy, A. R. (2024). Using Various Models for Predicting Soil Organic Carbon Based on DRIFT-FTIR and Chemical Analysis. Soil Systems, 8(1), 22.

Wang W, Zhang D, Kong H, Zhang G, Shen F, Huang Z. (2024). Effects of Salinity Accumulation on Physical, Chemical, and Microbial Properties of Soil under Rural Domestic Sewage Irrigation. Agronomy;14(3):514. https://doi.org/10.3390/agronomy14030514

Zaman, M., Shahid, S. A., Heng, L., Shahid, S. A., Zaman, M., and Heng, L. (2018). Soil salinity: Historical perspectives and a world overview of the problem. Guideline for salinity assessment, mitigation and adaptation using nuclear and related techniques, 43-53.